Facile Fabrication of Robust and Fluorine-Free Superhydrophobic PDMS/STA-Coated Cotton Fabric for Highly Efficient Oil-Water Separation

Enzhou Liu * and Daibin Tang

Posted Date: 14 April 2023

doi: 10.20944/preprints202304.0357.v1

Keywords: PDMS; STA; Superhydrophobic cotton fabric ; Oil-water separation; High separation flux

Article

Facile Fabrication of Robust and Fluorine-Free Superhydrophobic PDMS/STA-Coated Cotton Fabric for Highly Efficient Oil-Water Separation

Daibin Tang and Enzhou Liu *

School of Chemical Engineering/Xi'an Key Laboratory of Special Energy Materials, Northwest University, Xi'an,710069, P. R. China

* Correspondence: liuenzhou@nwu.edu.cn

Abstract: Oil-water separation using special wettability materials has received much attention due to its low energy consumption and high separation efficiency. Herein, a fluorine-free superhydrophobic cotton fabric(PDMS/STA -coated cotton fabric) was successfully prepared by a simple impregnation method using hydroxyl-capped polydimethylsiloxane (PDMS-OH), tetraethoxysilane (TEOS) and stearic acid (STA) as precursors. The Investigation found that the cross-linking reactions between the hydroxyl groups form PDMS-OH, hydrolyzed TEOS made a strong interact of PDMS-OH and cotton fabric. Besides, a suitable roughness surface of coated cotton fabric was established by introducing STA due to its long chain-structure. The contact angle of this composite can reach 158.7°under optical condition due to its low surface energy and desired roughness. The oil/water separation efficiency of PDMS/STA-coated cotton fabric is higher than 90% even after 10 cycles of oil-water separation, the oil flux can reach 11862.42 L m^{-2} h^{-1}. In addition, PDMS/STA-coated cotton fabric exhibits excellent chemical stability and durability under extreme conditions such as strong acid (HCl, pH = 1~2) and alkali (NaOH, pH = 13~14), the hydrophobicity of PDMS/STA-coated cotton fabric was decreased to 147° even after 350 cycles of abrasion testing.

Keywords: PDMS; STA; superhydrophobic cotton fabric; oil-water separation; high separation flux

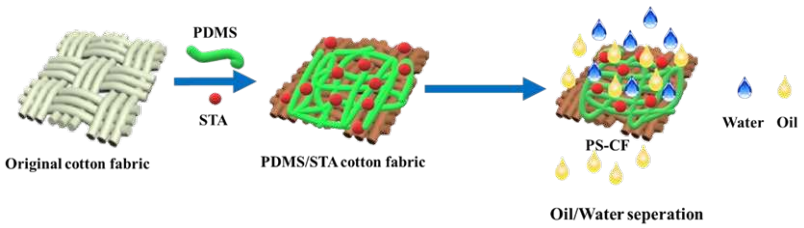

Graphical Abstract

1. Introduction

The production processes of industries are accompanied by the releasing amount of wastewater containing oil [1,2]. Meanwhile, the frequent occurrence of oil spills in recent years has caused severe environmental issues [3,4]. In extreme cases, these oily wastewaters can threaten the ecological environment and human health if they are not treated properly and promptly [5,6]. Currently, mechanical extraction [7], chemical degradation [8], combustion [9], and physical adsorption [10] are the most prevalent methods for dealing with oil-water separation problem. Although they can alleviate above pollution to some extent, the high cost, secondary pollution, low separation efficiency and poor reusability have serious limited their large-scale applications. Recently, porous materials such as sponges, foams, and textiles are employed to absorb oil from the wastewater [11–16]. However, the capacity and flux are typically low because these materials themselves do not

discriminate between water and oil, resulting in an unsatisfactory separation selectivity and efficiency. Therefore, it is urgent to explore an oil-water separation material with low energy cost, high efficiency, long-term stability, and environmentally friendly features.

Since the discovery of the lotus leaf effect [17], superhydrophobic materials with high water repellency abilities can achieve self-cleaning [18], anti-corrosion [19], anti-biofouling [20], anti-fogging [21] and oil-water separation [22], and so on. Preparation of superhydrophobic materials with oil-water separation ability have become a research topic. There are numerous methods for fabricating superhydrophobic materials, including spraying [23–26], impregnation [27–29], sol-gel [30–32], etching [33,34], and (electro)chemical deposition [35–37], etc. Typically, substances with low surface energy, such as, fluorinated silanes [38], tetrafluoroethylene [39], fluoropolymer [40,41] were used to reduce the surface energy and enhance the roughness of systems in order to obtain superhydrophobic materials. For example, Lin [42] reported a dual-functional superhydrophobic photothermal coating on glass by a chemical vapor deposition method, which was obtained by using candle soot (CS) and 1 H, 1 H, 2 H, 2 H-perfluorodecyltrimethoxysilane (PFDTMS) as row materials, coating exhibited superhydrophobic and great antibacterial and anti-biofilm formation Performance. Chen [43] fabricated a superhydrophobic 316L stainless-steel mesh by using perfluorooctanoic acid as low energy materials through an anodic oxidation method, the separation efficiency of various oils was above 95%, etc. However, these fluorine-containing materials are usually costly, complex fabrication process and existence secondary contamination [44]. Therefore, exploration fluorine-free materials had received much attention. Tagliaro [45] reported a sustainable fluorine-free transparent coating, which was obtained by modification with fatty acid side groups and then deposited through a solvent-free deposition method, showing good durability with high hydrophobicity. Ahmad N [46] prepared a TiO_2-APTES-superhydrophobic cotton fabrics by using aminopropyltriethoxysilane (APTES) coupling agent through an immersion method for oil/water separation, the modified cotton fabric shows more than 95 % oil–water separation efficiency for various types of oils ,and it has good mechanical and chemical durability. But as most of superhydrophobic material preparation processes, the cases mentioned above typically involve complex preparation processes and costly specialized equipment, limiting their practical application [47–51]. Considering industrial production, the impregnation processes are regarded as the most promising methods for preparation superhydrophobic materials due to its simple requirements [52–54]. Meanwhile, as a low-cost, high-yield natural fiber, cotton fabric is widely used in industries for its comfort, softness, breathability, wash resistance, and moisture absorption properties [55–57]. Thus, it is essential to combine their benefit.

Herein, a robust fluorine-free superhydrophobic cotton fabric is prepared by a simple impregnation process using polydimethylsiloxane (PDMS-OH) and stearic acid (STA) as precursors. The hierarchical surface structure of cotton fabric not only increases the fabric's roughness, but also captures air to form air cushion between the coating and the water. In addition, cross-linking reaction between the hydroxyl group of PDMS-OH and tetraethoxysilane (TEOS) during the condensation reaction can further strengthen the connection between the superhydrophobic coating and the cotton fabric. The obtained superhydrophobic cotton fabric has excellent resistance durability, chemical stability, self-cleaning performance, and a high oil-water separation efficiency with a desired separation flux.

2. Materials and Methods

2.1. Materials

Hydroxyl-terminated polydimethylsiloxane (PDMS-OH, cst = 40) was purchased from Macklin reagent Co., Ltd. (China). Tetraethoxysilane(TEOS, AR) was obtained from Damao chemical reagent factory, bis(lauroyloxy)dioctyltin(DOTDL, 96%) was received from Shanghai Yien Chemical Technology Co., Ltd., stearic acid (STA, CP), n-hexane(AR), anhydrous ethanol (AR) were provided by Tianjin Fuyu Fine Chemical Co., Ltd. methylene blue (MB), rhodamine B (Rh B) were purchased from Beijing Chemical Works. Sandpaper (360 meshes), peanut oil and cotton fabric (CF) were bought

Preprints (www.preprints.org) | NOT PEER-REVIEWED | Posted: 14 April 2023 doi:10.20944/preprints202304.0357.v1

from a local market. All chemicals were used as received without further purification, and ultra-pure water was used during all experiments. The pristine CF was ultrasonically cleaned with anhydrous ethanol and water in order to remove the surface impurities, and then dried in an oven for further procedures.

2.2. Fabrication of superhydrophobic cotton fabric

Figure 1 shows the fabrication processes of superhydrophobic cotton fabric. Specifically, 1.0 g PDMS and 4.0 g TEOS were added into 30 mL n-hexane solution for cross-linking with the assistance of 0.1 g bis(lauroyloxy)dioctyltin (DOTDL) catalyst at room temperature for 4 h. Subsequently, appropriate stearic acid was heated at 75 ℃ in 40 mL n-hexane until it was dissolved completely. Then, the pretreated CF (60 mm × 60 mm) was immersed in the above mixture for 24 h. Finally, the coated-CF was dried at 60°C to obtain superhydrophobic PDMS/STA-coated cotton fabric (PS-CF). Besides, PDMS-OH and STA were used respectively to treat CF under the same condition, the products were marked as P-CF and S-CF.

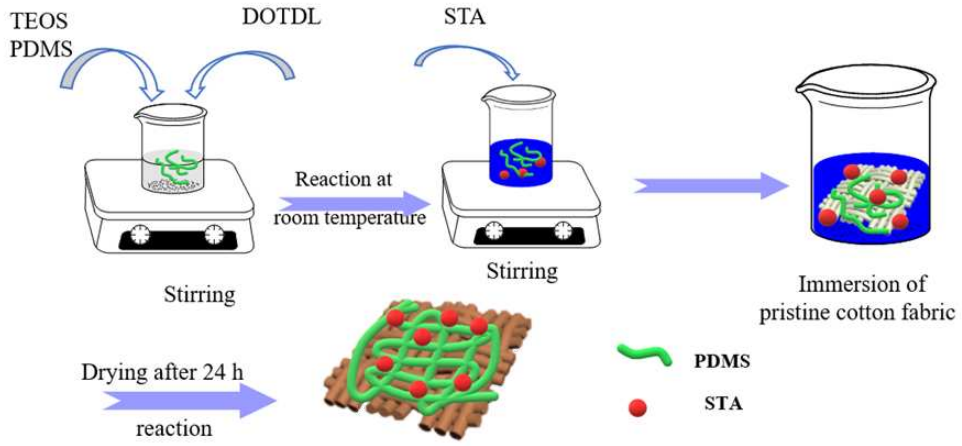

Figure 1. Preparation processes of PDMS/STA-coated CF.

2.3. Characterizations

The water contact angle (WCA) was carried out using a Contact Angle System OCA20 (Dataphysics, Germany) with 2~3 uL deionized water at room temperature. The WCA was the average of three different positions of the samples. X-ray photoelectron spectroscopy (XPS, Kratos AXIS NOVA spectrometer) and Fourier transform infrared spectra (FT-IR, PerkinElmer Frontier) were employed to reveal the chemical composition of the samples. The morphologies of samples were observed by the scanning electron microscope (SEM, Carl Zeiss SIGMA) coupled with X-ray energy dispersive spectrometer (EDS).

3. Results and discussion

3.1. Wettability of superhydrophobic cotton fabric

Figure 2(a, b) shows the states of various liquids on the surface of superhydrophobic PDMS/STA-coated cotton fabric and original cotton fabric. It can be observed that the water-based liquid droplets on the composite are spherical, including milk, tea and juice, the oils such as n-hexane, dichloromethane are in a completely saturated state. As shown in Figure 2(c), when the tilt angle of the fabric is less than 10°, the water droplets can slide down the PS-CF surface quickly, indicating that the cotton fabric prepared in this work has superhydrophobic properties. It is known from the Cassie–Baxter equation that this non-wetting phenomenon results from the low adhesion caused by the air cushion, which makes the water droplets to easily roll off the surface of the PS-CF. Then, the PS-CF was immersed into the water (Figure 2d), the phenomenon of 'silver mirror' can be observed over the surface of PS-CF, which results from a large number of air pockets created by the micro-

Preprints (www.preprints.org) | NOT PEER-REVIEWED | Posted: 14 April 2023 doi:10.20944/preprints202304.0357.v1

nano structure on the surface of PS-CF, suggesting that the above superhydrophobic phenomenon belongs to Cassie-Baxter state [58].

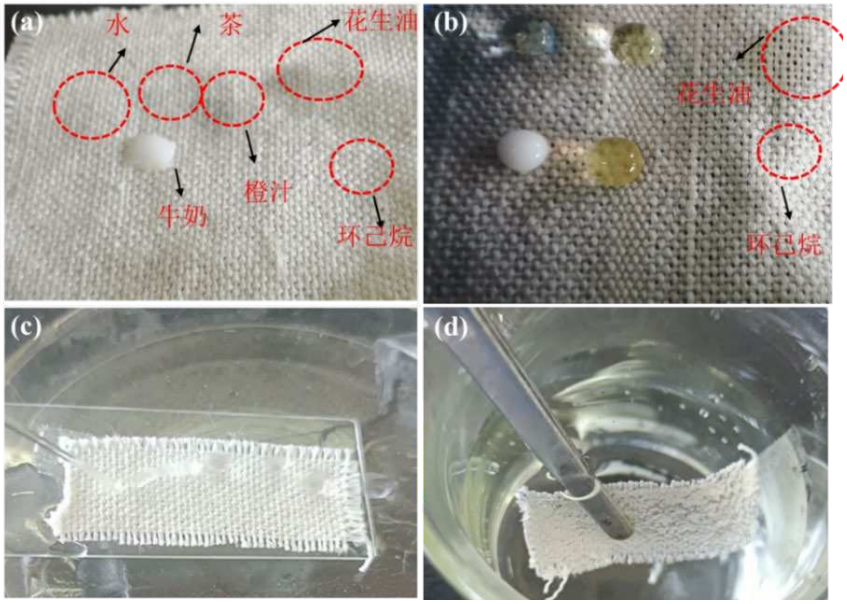

Figure 2. Images of (a) liquid droplets on the CF, (b) liquid droplets on PS-CF and (c) water rolling off from the surface of PS-CF and (d) PS-CF in water.

3.2. Formation of superhydrophobic PDMS/STA-coated cotton fabric

Due to the presence of large number of hydroxyl groups on cellulose, the primary component of cotton fabric, the original cotton fabric is hydrophilic with WCA lower than 90o. In this work, PDMS-OH and STA were used to reduce the surface energy of cotton fabric with an appropriate roughness. The silane coupling agent TEOS was employed to cross-link with PDMS-OH to form an irregular mesh structure on the surface of cotton fabric under the assistance of DOTDL, hydrolyzed TEOS, PDMS-OH and cotton fabric can form strong connections by the condensation reaction.

FT-IR spectroscopy was used to determine the chemical compositions of untreated cotton fabric and PDMS/STA-coated superhydrophobic cotton fabric. As shown in Figure 3(a), the peak at 3334 cm^{-1} from untreated cotton fabric corresponds to the stretching vibrations of –OH, and peaks at 2914 and 2851 cm^{-1} stem from $–CH_2$ symmetrical stretching vibrations. Moreover, a strong peak at 1026 cm^{-1} is associated with –OH bending vibration and C–O–C stretching vibration. For the PDMS/STA-coated superhydrophobic cotton fabric, a new peak at 2964 cm^{-1} corresponds to the stretching vibration of the $–CH_3$ group from PDMS-OH, indicating PDMS is successfully deposited on the surface of cotton fabric. The signal at 1260 cm^{-1} belongs to the $–CH_3$ stretching vibration from $Si–CH_3$, further indicating the presence of PDMS-OH elastomer [59]. In addition, a new peak at 794 cm^{-1} originates from the Si–O–Si symmetric stretching vibration in the composite. The peak at 1697 cm^{-1} is associated with C=O stretching, confirming the successful implementation of STA. Besides, the peak intensity at 3334 cm^{-1} is clearly reduced, implying the surface –OH groups is consumed by the cross-linking reaction with PDMS-OH and hydrolyzed TEOS [60]. Furthermore, EDS was utilized to analyze the surface chemical composition of the composite. C (51.94 wt%), O (40.16 wt%) and Si (7.9 wt%) were evenly distributed on the surface of the PDMS/STA-coated cotton fabric in Figure 3(b). The above results indicate that the cotton fabric coated with PDMS and STA was successfully fabricated.

Preprints (www.preprints.org) | NOT PEER-REVIEWED | Posted: 14 April 2023 doi:10.20944/preprints202304.0357.v1

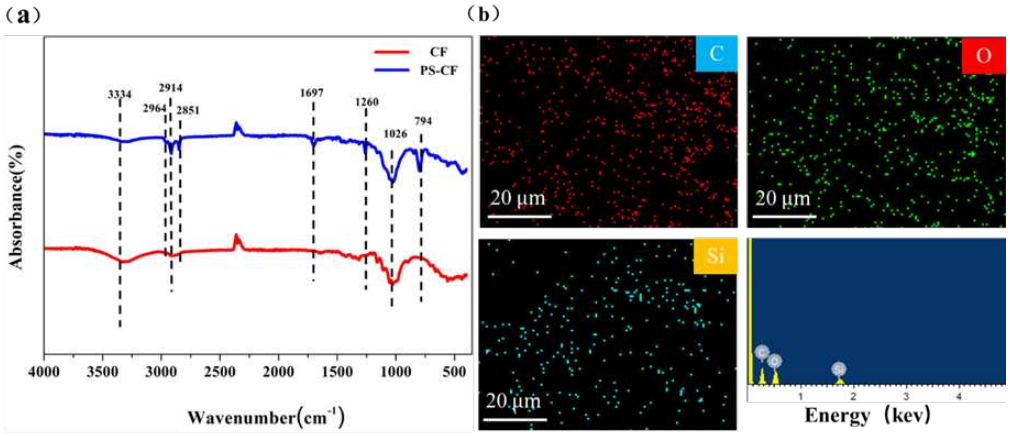

Figure 3. (a) FT-IR spectra of CF and PS-CF, (b) Element distribution map and curve of PS-CF.

Figure 4 presents the XPS spectra of the samples. The survey spectrum implies that the pristine cotton fabric is consisted of elements C and O in Figure 4(a). After introducing PDMS-OH, TEOS and STA, a new Si signal belonging to Si 2*s* and Si 2*p* is detected at 153.08 eV and 102.08 eV in Figure 4(b). Moreover, the content of O element on the surface of PS-CF increases substantially and the content of C element decreases. This is due to the large amount of -COOH in STA, which leads to a corresponding increase of O element. This result further proves that the PS-CF surface is covered by the cross-linked network formed by PDMS and STA. Besides, the high-resolution XPS C1s and Si 2*p* spectra of the samples were studied. The C1*s* of CF can be curve-fitted into typical peaks of C-O, C=O and C-C with binding energies at 288.7, 286.1 and 284.8 eV, respectively. As shown in Figure 4(c, d), the intensity of C=O and C-O groups in the composite increases after introducing PDMS/STA coating, which is consistent with FT-IR analysis. Comparing the Si 2*p* high-resolution profiles of the CF and PS-CF in Figure 4(e, f), it can be seen that the orbital peaks located at 102.28 eV and 103.78 eV are attributed to the Si-C and Si-O-Si bonds, respectively. The above results indicate the successful loading of PDMS and STA on the surface of cotton fabrics.

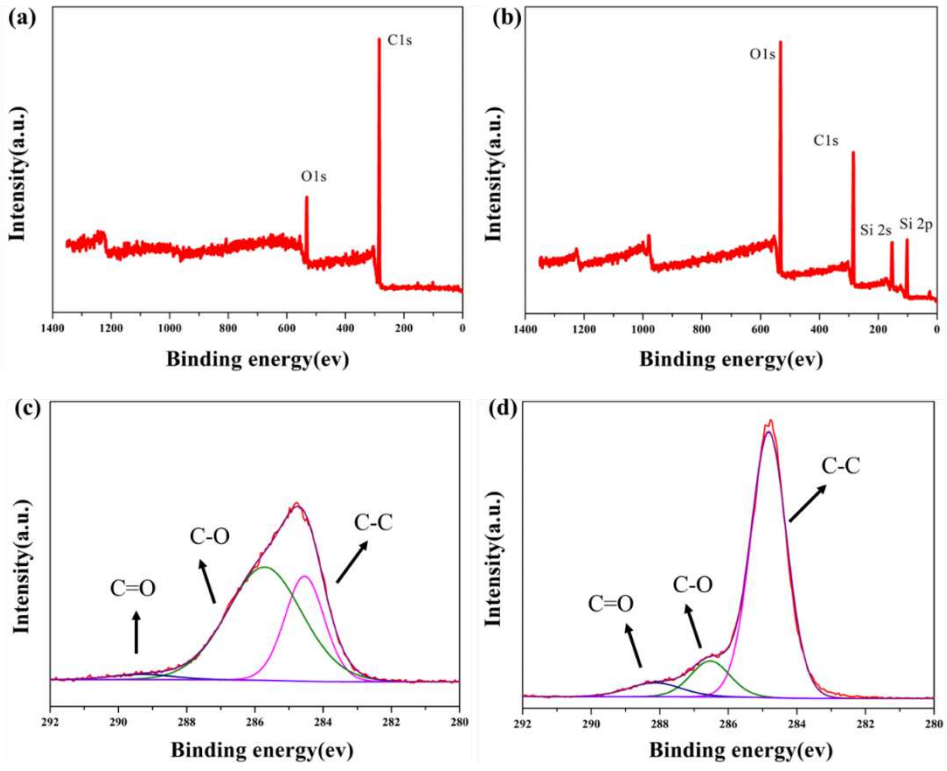

Preprints (www.preprints.org) | NOT PEER-REVIEWED | Posted: 14 April 2023 doi:10.20944/preprints202304.0357.v1

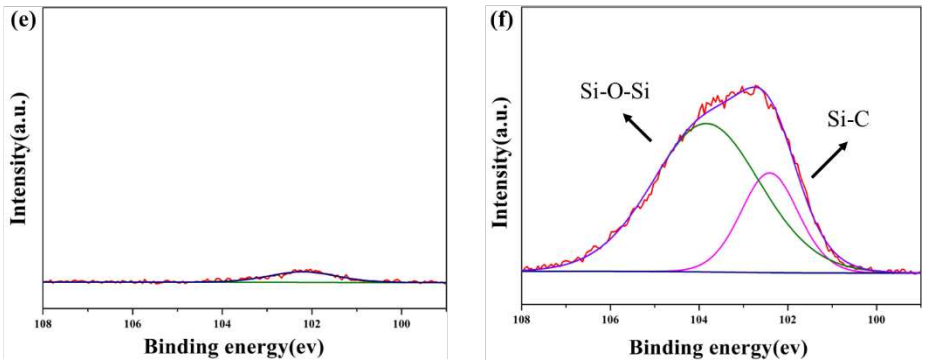

Figure 4. (a, b) XPS survey spectra, (c, d) high-resolution spectra of C1*s* and (e, f) high-resolution spectra of Si 2*p* of CF and PS-CF sample.

In order to further investigate the relationship between the surface micromorphology and material wettability of CF, PCF, SCF and PS-CF, the surface micromorphology of samples was observed by SEM. Figure 5(a) shows the SEM image of the original cotton fabric, it is relatively smooth overall with fine protrusions distributed on the cotton fabric fibers. Figure 5(b) is the SEM image of PCF, which was treated with PDMS-OH only, compared with the original cotton fabric, its surface is obviously smoother and flatter, a layer of film-like material is uniformly attached to the surface of the fabric fibers, and the texture of the original cotton fabric fibers is reduced. This is due to the uniform film formed by the cross-linking reaction between PDMS-OH and TEOS on the surface of the cotton fabric, which reduces the surface tension of the fabric [44]. Figure 5(c) shows the surface of the SCF sample treated with STA only, the fabric surface is obviously rough compared to CF and PCF, STA is unevenly distributed on the fabric surface, the fabric fiber protrusions increase and some fibers are broken. This is because STA is simply attached to the surface of cotton fabric and not firmly. As shown in Figure 5(d), the protrusions on the fabric fiber surface flat and protruding significantly more, STA on the fabric surface shows flower morphology, and STA is more uniformly distributed on PS-CF samples compared to SCF, the overall roughness of the fabric increases significantly. The WCA of 132°, 138° and 154° of water droplets on PCF, SCF and PS-CF, respectively. It shows that the synergistic effect of PDMS and STA satisfies the low surface energy and suitable roughness required for building superhydrophobic surface materials.

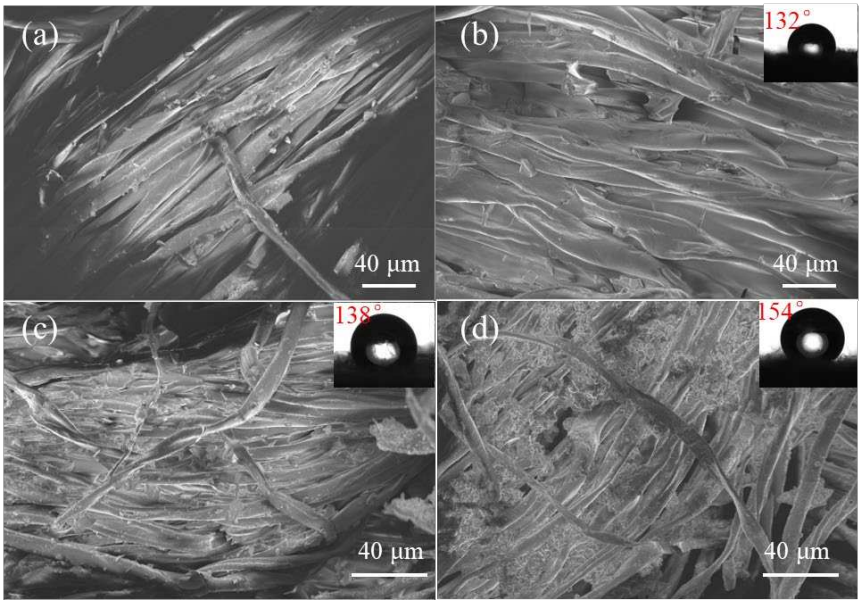

Figure 5. SEM images of (a) CF, (b) PCF, (c) SCF and (d) PS-CF.

3.3. Oil-water separation

Preprints (www.preprints.org) | NOT PEER-REVIEWED | Posted: 14 April 2023 doi:10.20944/preprints202304.0357.v1

Figure 6 shows the schematic illustration of oil/water separation device and process. The oil-water mixture contains 50 mL of water and 50 mL of different oil, including dichloromethane, trichloromethane cyclohexane, peanut oil, n-hexane. The oil and water were pre-stained with rhodamine B(Rh B) and methylene blue (MB) for clear observation, respectively. The oil-water separation experiment was conducted by laying the prepared PS-CF at the mouth of the oil-water separation device(25 mm × 25 mm). The oil-water mixture is poured into the above device, and the separation process is conducted under the help of gravity. Additionally, the time for the whole separation process and the amount of separated oil are recorded. After each cycle, the PS-CF was washed with anhydrous ethanol and deionized water, then dried at 60 °C before the next separation cycle.

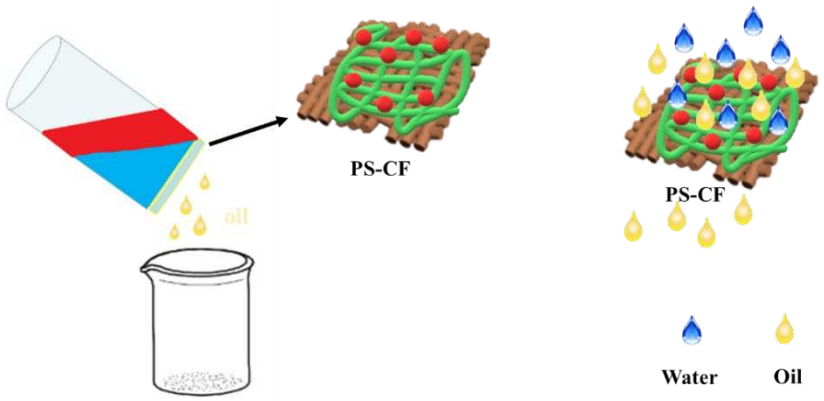

Figure 6. Schematic illustration of oil/water separation device and process.

The oil-water separation efficiency(*Es*) is defined as follows:

$$E_S = \frac{V_a}{V_b} \times 100\%$$

Where V_a represents the volume of the oil before the separation process and V_b represents the volume of the oil after the separation process.

Formula for calculating the permeate flux(***J***) during the oil-water separation of various types oils is as follows:

$$J = \frac{V}{S \times T}$$

Where V(L) represents the total volume of oil penetrated, S(m²) represents the effective penetration area during oil-water separation, T(h) represents the duration of the oil-water separation process.

Due to the PS-CF has superhydrophobic and lipophilic properties, that enable it to be used in the field of oil-water separation. When the oil-water mixture passes through the oil-water separation device with PS-CF as the filter membrane under the action of gravity, the water phase is trapped above the fabric, while the oil phase can wet the PS-CF and pass through the membrane, thus realizing the separation of oil and water phases. Oil-water separation experimental results are shown in Figure 7(a), separation efficiency of dichloromethane/water mixing system is 98.2%, trichloromethane/water system separation efficiency is 97%, n-hexane/water system and cyclohexane/water system results are closer, respectively, 93.2% and 93.8%, the separation efficiency of the peanut oil/water mixed system was only 90.4%. On the one hand, dichloromethane and trichloromethane, as representatives of heavy oils, are denser than water, and dichloromethane and trichloromethane are more likely to penetrate through the aqueous phase layer and thus through the PS-CF filter layer under gravity than peanut oil, n-hexane and cyclohexane, which are lighter in density than water. On the other hand, the difference in viscosity and physicochemical properties of

Preprints (www.preprints.org) | NOT PEER-REVIEWED | Posted: 14 April 2023 doi:10.20944/preprints202304.0357.v1

the oils, peanut oil is more viscous than the other four oils, which is more likely to be adsorbed in the pores of the substrate when passing through the cotton fabric as the porous substrate material, making the pores of the substrate smaller or even blocked, resulting in a lower separation efficiency and permeation flux of different oil.

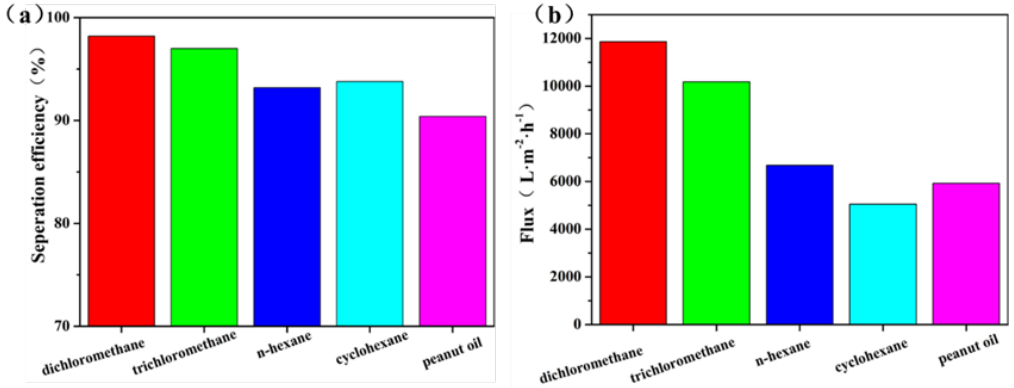

Figure 7. (a) the separation efficiencies and (b)the flux of oil during oil-water separation.

The oil flux is another significant indicator for evaluating the oil-water separation process. Therefore, five different oil's fluxes on PS-CF were measured. Heavy oil and light oil had different separation fluxes due to their different density, as shown in Figure 7(b), the permeate fluxes of dichloromethane and trichloroformethane can reach 11862.42 $L{\cdot}m^{-2}{\cdot}h^{-1}$and 9320.71 $L{\cdot}m^{-2}{\cdot}h^{-1}$, respectively, and the permeate fluxes of peanut oil, n-hexane, and cyclohexane in water were 4926.67, 5921.55, and 6680.73 $L{\cdot}m^{-2}{\cdot}h^{-1}$, respectively. Zhang [61] fabricated a superhydrophobic cotton by beeswax/lignin compound through spraying method, it can absorb oil form oil/water mixture, and the recovery rate of modified cotton for trichloromethane/water separation reaches at least 88.92% and the highest is 93.78%.Wen [62] using graft polymerization method to graft polymer brushes on the cotton surface for the immobilization of Ag, and which was subsequently coated with PDMS, the coated cotton fabric can separate oil from pure water and artificial seawater, the separation efficiency is 97%. Li [63] using fluorosurfactant to modify hydrophilic Al_2O_3 nanoparticles by mixing in ethanol solution, and then cotton fibers were immersed in above solution to get coated, as coated cotton fibers, the efficiency is higher than 98% of both diesel-in-water and hexadecane-in-water separation with 520 $L{\cdot}m^{-2}{\cdot}h^{-1}$ to 650 $L{\cdot}m^{-2}{\cdot}h^{-1}$ oil permeate flux. Therefore, PS-CF has relatively high separation efficiency and oil permeate flux.

In addition, PS-CF performs well in the oil-water separation cycle experiment. The dichloromethane/water system was chosen to conduct the cycle experiment, and the results are depicted in Figure 8. Although the overall oil-water separation efficiency decreases with increasing cycle times, the oil-water separation efficiency of the superhydrophobic cotton fabric can be maintained at 92.8% after 10 cycles.

Preprints (www.preprints.org) | NOT PEER-REVIEWED | Posted: 14 April 2023 doi:10.20944/preprints202304.0357.v1

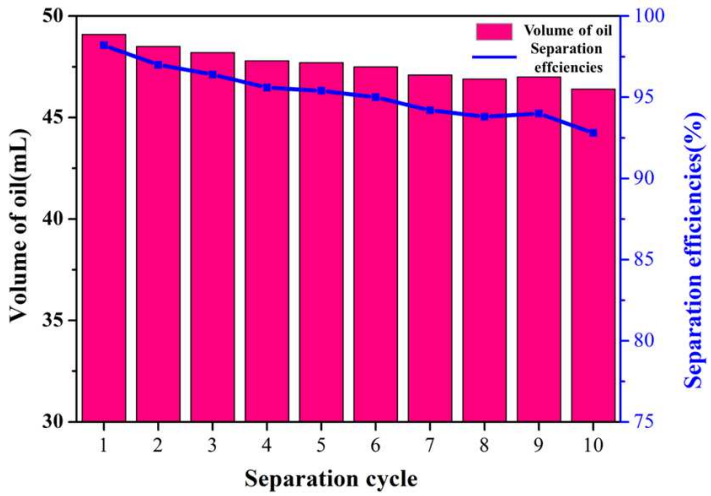

Figure 8. Association between separation efficiency and the number of cycles dichloromethane/water.

3.4. Durability and chemical stability of PS-CF

Superhydrophobic fabrics are unavoidably required for applications in harsh environments, therefore, superhydrophobic materials should withstand harsh conditions. Several sets of experiments have been designed in order to verify the usability of PS-CF in extreme conditions. As shown in Figure 9(a, b), to investigate the mechanical stability, we laid the sandpaper flat on the experimental table, attached the PS-CF to one side of the slide with double-sided tape, put a 150 g weight on the other side of the slide, and then moved the slide in the horizontal direction by traction for 10 cm. This process was regarded as one abrasion cycle. After 350 cycles of abrasion, the PS-CF remains superhydrophobic with WCA higher than 150° in Figure 9(c), whereas after 350 cycles of abrasion and beyond, the as-cotton fabric still maintains a good water repellency. Figure 9(c) displays the WCA of after abrasion test, inset is the SEM of fabric after 400 abrasion cycles, the WCA of PS-CF is 146.4°, indicating that PS-CF still has good mechanical strength due to the cross-linking network structure and the strong binding force between PDMS, STA and chemical bonds formed on the surface of cotton fabric.

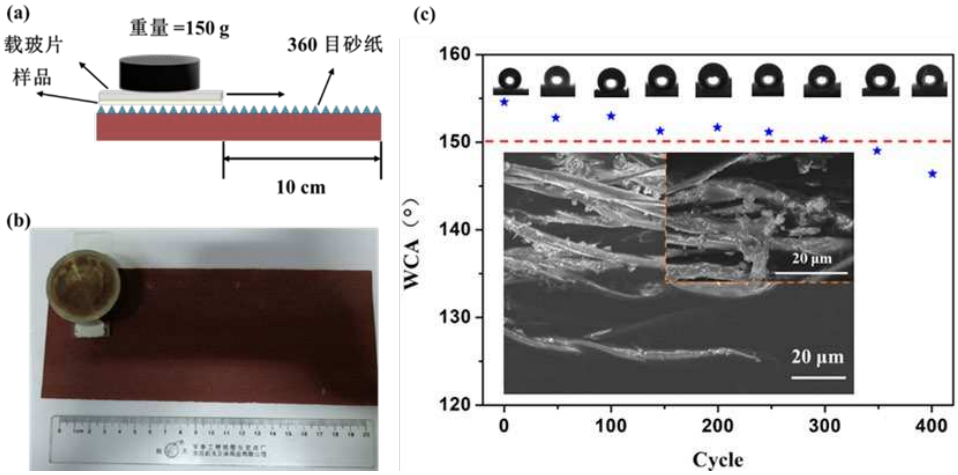

Figure 9. (a, b) Schematic of mechanical durability tests, (c) WCA of different abrasion cycles (inset is SEM image after abrasion cycles of 400).

As a material for oil-water separation applications, PS-CF will inevitably face scenarios where it is applied in extreme environments. Therefore, PS-CF should have good physicochemical stability, the chemical stability of PS-CF was tested. After the PS-CF fabric was completely immersed in deionized water, strong alkali solution (NaOH, pH=13~14), ethanol solution and strong acid solution

Preprints (www.preprints.org) | NOT PEER-REVIEWED | Posted: 14 April 2023 doi:10.20944/preprints202304.0357.v1

(HCl, pH=1~2) for a certain time, the WCA of the sample was measured after washing and drying with deionized water. Figure 10 shows the graphs of the changes of WCA on the surface of PS-CF after immersion in strong acid, strong base, ethanol and deionized water for 12, 24, 36, 48 and 72 h. The WCA of PS-CF decreases to 150.7° and 150.2° after immersion in water and NaOH solutions for more than 72 h. It still has the superhydrophobic property. In contrast, the WCA of PS-CF after immersion in ethanol and HCl solutions gradually decreases, and after 36 h immersion, the WCA of the samples is lower than 150°, and the WCA of PS-CF samples are 142.2° and 140.5° after 72 h immersion, it loses the superhydrophobicity but keeps good hydrophobicity.

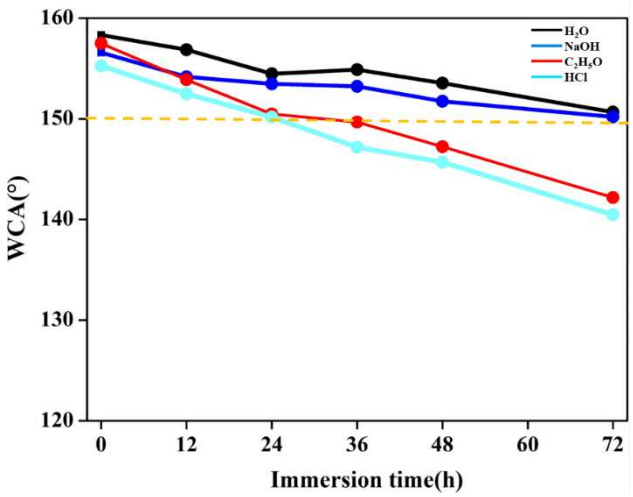

Figure 10. WCA change with time after PS-CF immersing in different solutions.

In order to further investigate the effect of different solutions on PS-CF, SEM characterization was performed on the samples after 72 h immersion. Figure 11(a, b, c, d) are the SEM images of the surface of PS-CF after immersion in deionized water, NaOH, ethanol and HCl for 72 h, respectively. As shown in Figure 11(a, b), the fabric fiber surface of the PS-CF samples did not change significantly after 72 h of immersing in deionized water and NaOH, and there was no obvious trace of damage to the micro- and nanostructure on its, so the samples could still maintain their superhydrophobic state after immersion. The fabric fiber surface of the PS-CF samples shown in Figure 11(c, d) after immersing in ethanol and HCl solution for 72 h obviously had less adhesion, and the surface was smoother and flatter compared with before, and the surface rough structure was damaged. This is because the cross-linked network formed by the condensation of silanol bonds and hydroxyl groups of PDMS-OH on the fabric surface was destroyed by the strong acidic HCl, resulting in the loss of strong bonding between the particles on the surface of the cotton fabric, as a result, some of the STA particles fell off, hydrophobic properties of the samples were reduced. With long time immersing in ethanol solution, some PMDS-OH and STA will be shed due to dissolution, However, in the ambient environment, the solubility of PDMS-OH and STA in ethanol solution is relatively low, consequently, the WCA on the surface of SPCF after immersing in ethanol solution for the same time is slightly higher than in HCl.

Preprints (www.preprints.org) | NOT PEER-REVIEWED | Posted: 14 April 2023 doi:10.20944/preprints202304.0357.v1

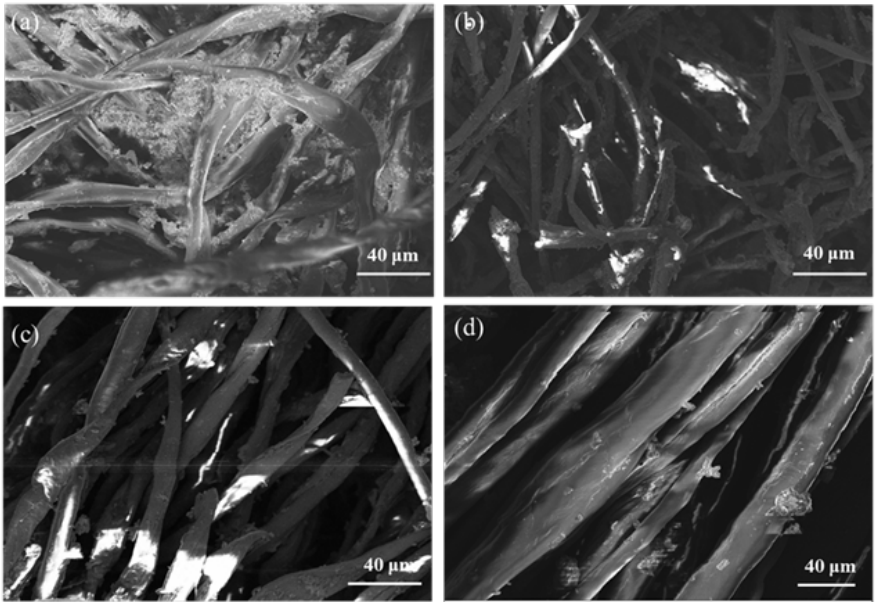

Figure 11. SEM images of PS-CF after 72 h immersed in (a) H_2O, (b) NaOH, (c) C_2H_5OH and (d) HCl.

The low surface energy substances used in the construction of superhydrophobic surface materials and the particulate materials or structures that provide roughness can be peeled off or destroyed during application due to vibration or other factors, resulting in a decrease within the hydrophobic properties of the materials. To estimate the peeling resistance of the material, ultrasonic peeling resistance testing was conducted on PS-CF.

Figure 12 shows the results of sonicating PS-CF adhered to a slide glass with double-sided adhesive and placed in an ultrasonic cleaner. After 12 h of sonication peeling, the SPCF had a WCA of 152,2° and still maintained superhydrophobic. This is because the PDMS-OH and STA on the surface of the fabric are chemically bonded, instead of being simple mechanically attached. Once again, the test results indicate that PS-CF has excellent durability.

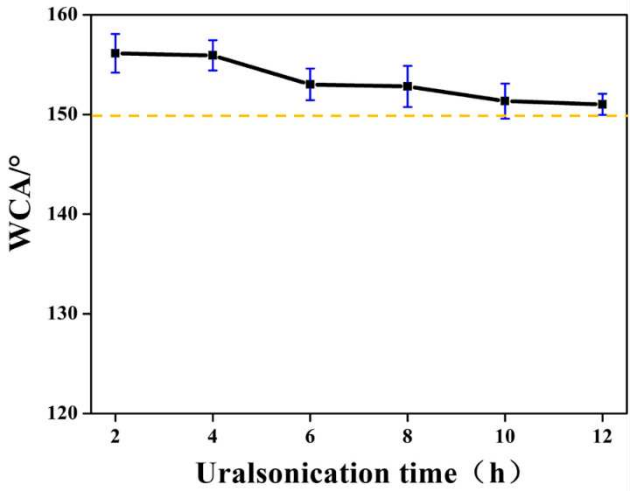

Figure 12. The relationship of WAC and ultrasonication time.

5. Conclusions

In summary, a superhydrophobic cotton fabric with great durability, fluorine-free and low cost was fabricated through impregnation method. Due to low-surface-energy material and hierarchical rough surface, the surface static water contact angle (WCA) of the superhydrophobic cotton fabric can reach 158.6°. Moreover, as-prepared PS-CF can maintain the superhydrophobicity in alkaline environments for over 72 h, withstand over 350 abrasion cycles. Additionally, the oil-water

separation efficiency of PS-CF is higher than 90% when it is applied to various oil-water mixed systems and maintains a better separation efficiency with high level flux of oil.

Acknowledgments: This work was supported by the National Natural Science Foundation of China (11974276 and 22078261), Natural Science Basic Research Program of Shaanxi Province (2023-JC-YB-111), Key Science and Technology Innovation Team of Shaanxi Province (2022TD-33).

Conflicts of Interest: The authors declare no conflict of interest.

References

1. McClenachan G, Turner R E. Disturbance legacies and shifting trajectories: Marsh soil strength and shoreline erosion a decade after the Deepwater Horizon oil spill[J]. *Environmental Pollution*, **2023**, *322*: 121151.
2. Postel S L, Daily G C, Ehrlich P R. Human appropriation of renewable fresh water[J]. *Science*, **1996**, *271*(5250): 785-788.
3. Ebenstein A. The consequences of industrialization: evidence from water pollution and digestive cancers in China[J]. *Review of Economics and Statistics*, **2012**, *94(1)*: 186-201.
4. Alves T M, Kokinou E, Zodiatis G, et al. Multidisciplinary oil spill modeling to protect coastal communities and the environment of the Eastern Mediterranean Sea[J]. *Scientific Reports*, **2016**, *6(1)*: 1-9.
5. Sharma J, Dean J, Aljaberi F, et al. In-situ combustion in bellevue field in louisiana–history, current state and future strategies[J]. *Fuel*, **2021**, *284*: 118992.
6. Li B, Liu X, Zhang X, et al. Stainless steel mesh coated with silica for oil–water separation[J]. *European Polymer Journal*, **2015**, *73*: 374-379.
7. Zhan M, Yang W, Zhang F, et al. Experimental investigation on the separation performance for a new oil-water separator[J]. *Frontiers in Energy Research*, **2021**, *8*: 608586.
8. Khan J A, Al-Kayiem H H, Aleem W, et al. Influence of alkali-surfactant-polymer flooding on the coalescence and sedimentation of oil/water emulsion in gravity separation[J]. Journal of Petroleum Science and Engineering, 2019, 173: 640-649.
9. Xiang B, Sun Q, Zhong Q, et al. Current research situation and future prospect of superwetting smart oil/water separation materials[J]. *Journal of Materials Chemistry A*, **2022**, *10(38)*: 20190-20217.
10. Baig U, Faizan M, Dastageer M A. Polyimide based super-wettable membranes/materials for high performance oil/water mixture and emulsion separation: A review[J]. *Advances in Colloid and Interface Science*, **2021**, *297*: 102525.
11. Yang Y, Guo Z, Liu W. Special Superwetting Materials from Bioinspired to Intelligent Surface for On--Demand Oil/Water Separation: A Comprehensive Review[J]. *Small*, **2022**,*18*: 2204624.
12. Baig U, Faizan M, Dastageer M A. Polyimide based super-wettable membranes/materials for high performance oil/water mixture and emulsion separation: A review[J]. *Advances in Colloid and Interface Science*, **2021**, *297*: 102525.
13. He Y, Li J, Luo K, et al. Engineering reduced graphene oxide aerogel produced by effective γ-ray radiation-induced self-assembly and its application for continuous oil–water separation[J]. *Industrial & Engineering Chemistry Research*, **2016**, *55(13)*: 3775-3781.
14. Sim I, Park S, Shin K Y, et al. Inkjet Printing of High Aspect Ratio Silver Lines via Laser-Induced Selective Surface Wetting Technique[J]. *Coatings*, **2023**, *13(4)*: 683.
15. Jia C, Zhu J, Zhang L. An Anti-Corrosion Superhydrophobic Copper Surface Fabricated by Milling and Chemical Deposition[J]. *Coatings*, **2022**, *12(4)*: 442.
16. Li A, Jia Y, Zhang F, et al. The Effects of Zinc Oxide/Silicon Dioxide Composite Coating on Surface Wettability and the Mechanical Properties of Paper Mulching Film[J]. *Coatings*, **2022**, *12(5)*: 555.
17. Barthlott W, Neinhuis C. Purity of the sacred lotus, or escape from contamination in biological surfaces[J]. *Planta*, **1997**, *202*: 1-8.
18. Peng J, Yuan S, Geng H, et al. Robust and multifunctional superamphiphobic coating toward effective anti-adhesion[J]. *Chemical Engineering Journal*, **2022**, *428*: 131162.
19. Zhang S, Li Y, Yang H, et al. Multifunctional superhydrophobic composite coatings with remarkable passive heat dissipation and anticorrosion properties[J]. *Industrial and Engineering Chemistry Research*, **2021**, *60(30)*: 11019-11029.

20. Al--Ahmed Z A, Alzahrani S O, AlJohani A K B, et al. An anticounterfeiting strategy based on photochromic nonwoven polyester fabric by plasma--assisting spray coating with ultraviolet--responsive silica@ strontium aluminate nanoparticles[J]. *Applied Organometallic Chemistry*, **2023**, *37(4)*: e7035.
21. Sharma J, Dean J, Aljaberi F, et al. In-situ combustion in bellevue field in louisiana–history, current state and future strategies[J]. *Fuel*, **2021**, *284*: 118992.
22. Wang W, Dong C, Liu S, et al. Super-hydrophobic cotton aerogel with ultra-high flux and high oil retention capability for efficient oil/water separation[J]. Colloids and Surfaces A: *Physicochemical and Engineering Aspects*, **2023**, *657*: 130572.
23. Abu Jarad N, Imran H, Imani S M, et al. Fabrication of superamphiphobic surfaces via spray coating; a review[J]. *Advanced Materials Technologies*, **2022**, *7(10)*: 2101702.
24. Li Y, Shi X, Bai W, et al. Robust superhydrophobic materials with outstanding durability fabricated by epoxy adhesive-assisted facile spray method[J]. Colloids and Surfaces A: Physicochemical and Engineering Aspects, 2023, 664: 131109.
25. Yang Z, Chang J, He X, et al. Construction of robust slippery lubricant-infused epoxy-nanocomposite coatings for marine antifouling application[J]. *Progress in Organic Coatings*, **2023**, *177*: 107458.
26. Li K, Xiang J, Zhou J, et al. Self-healing and wear resistance stable superhydrophobic composite coating with electrothermal and photothermal effects for anti-icing[J]. *Progress in Organic Coatings*, **2023**, *177*: 107415.
27. Camalan M, Arol A İ. Preliminary assessment of spray coating, solution-immersion and dip coating to render minerals superhydrophobic[J]. *Minerals Engineering*, **2022**, *176*: 107357.
28. Xia Y, Fan G, Chen K, et al. Preparation and anti-corrosion performances of grass-like microstructured superhydrophobic surface on copper via solution-immersion[J]. *Materials Letters*, **2022**, *323*: 132482.
29. Liao C, Li Y, Gao M, et al. Bio-inspired construction of super-hydrophobic, eco-friendly multifunctional and bio-based cotton fabrics via impregnation method[J]. *Colloids and Surfaces A: Physicochemical and Engineering Aspects*, **2022**, *651*: 129647.
30. Duan Y, Wu J, Qi W, et al. Eco-friendly marine antifouling coating consisting of cellulose nanocrystals with bioinspired micromorphology[J]. *Carbohydrate Polymers*, **2023**, *304*: 120504.
31. Ren C, Yu Y. Superhydrophobic, heat-resistant alumina-methylsilsesquioxane hybrid aerogels with enhanced thermal insulating performance in high humidity[J]. *Ceramics International*, **2023**, *49(8)*: 12625-12632.
32. Zhang X, Si Y, Mo J, et al. Robust micro-nanoscale flowerlike ZnO/epoxy resin superhydrophobic coating with rapid healing ability[J]. *Chemical Engineering Journal*, **2017**, *313*: 1152-1159.
33. Zhu S, Deng W, Su Y. Recent advances in preparation of metallic superhydrophobic surface by chemical etching and its applications[J]. *Chinese Journal of Chemical Engineering*, **2023**. *in press.*
34. Xue Y, Wang Y, Wang Y, et al. Functionalized superhydrophobic MWCNT/PEI nanocomposite film with anti-icing and photo-/electrothermal deicing properties[J]. *Materials Chemistry and Physics*, **2023,** *297*: 127385.
35. Han J, Liu E, Zhou Y, et al. Robust superhydrophobic film on aluminum alloy prepared with TiO_2/SiO_2-silane composite film for efficient self-cleaning, anti-corrosion and anti-icing[J]. *Materials Today Communications*, **2023**, *34*: 105085.
36. Chu Z, Feng Y, Xu T, et al. Magnetic, self–heating and superhydrophobic sponge for solar–driven high–viscosity oil–water separation[J]. *Journal of Hazardous Materials,* **2023**, *445*: 130553.
37. Ouyang Y, Huang Z, Fang R, et al. Silica nanoparticles enhanced polysiloxane-modified nickel-based coatings on Mg alloy for robust superhydrophobicity and high corrosion resistance[J]. *Surface and Coatings Technology*, **2022**, *450*: 128995.
38. Jia C, Zhu J, Zhang L. An Anti-Corrosion Superhydrophobic Copper Surface Fabricated by Milling and Chemical Deposition[J]. *Coatings*, **2022**, *12(4):* 442.
39. Wang K, Dong Y, Zhang W, et al. Preparation of stable superhydrophobic coatings on wood substrate surfaces via mussel-inspired polydopamine and electroless deposition methods[J]. *Polymers*, **2017**, *9(6)*: 218.
40. Jeong H, Baek S, Han S, et al. Chemically Robust Superhydrophobic Poly (vinylidene fluoride) Films with Grafting Crosslinkable Fluorinated Silane[J]. *Macromolecular Research*, **2018**, *26*: 493-499.
41. Pathak P, Grewal H S. Solvent-free synthesis of superhydrophobic materials with self-regenerative and drag reduction properties[J]. *Colloids and Surfaces A: Physicochemical and Engineering Aspects*, **2023**, *658*: 130675.

42. Peng Z, Song J, Gao Y, et al. A fluorinated polymer sponge with superhydrophobicity for high-performance biomechanical energy harvesting[J]. *Nano Energy*, **2021**, *85*: 106021.
43. Lin Y, Zhang H, Zou Y, et al. Superhydrophobic photothermal coatings based on candle soot for prevention of biofilm formation[J]. *Journal of Materials Science & Technology*, **2023**, *132*: 18-26.
44. Chen Z, Zuo J, Zhao T, et al. Superhydrophobic copper foam bed with extended permeation channels for water-in-oil emulsion separation with high efficiency and flux[J]. *Journal of Environmental Chemical Engineering*, **2023**, *11(1)*: 109018.
45. Anitha C, Mayavan S. Salvinia inspired fluroine free superhydrophobic coatings[J]. *Applied Surface Science*, **2018**, *449*: 250-260.
46. Tagliaro I, Seccia S, Pellegrini B, et al. Chitosan-based coatings with tunable transparency and superhydrophobicity: A solvent-free and fluorine-free approach by stearoyl derivatization[J]. *Carbohydrate Polymers*, **2023**, *302*: 120424.
47. Ahmad N, Rasheed S, Ahmed K, et al. Facile two-step functionalization of multifunctional superhydrophobic cotton fabric for UV-blocking, self cleaning, antibacterial, and oil-water separation[J]. *Separation and Purification Technology*, **2023**, *306*: 122626.
48. Suryaprabha T, Sethuraman M G. Fabrication of a superhydrophobic and flame-retardant cotton fabric using a DNA-based coating[J]. *Journal of Materials Science*, **2020**, *55*: 11959-11969.
49. Li S, Yu L, Xiong J, et al. Facile Fabrication of Superhydrophobic and Flame-Retardant Coatings on Cotton Fabrics[J]. *Polymers*, **2022**, *14(23)*: 5314.
50. Ejeta D D, Wang C F, Kuo S W, et al. Preparation of superhydrophobic and superoleophilic cotton-based material for extremely high flux water-in-oil emulsion separation[J]. *Chemical Engineering Journal*, **2020**, *402*: 126289.
51. Li L, Li B, Sun H, et al. Compressible and conductive carbon aerogels from waste paper with exceptional performance for oil/water separation[J]. *Journal of Materials Chemistry A*, **2017**, *5(28)*: 14858-14864.
52. Yin Z, Pan Y, Bao M, et al. Superhydrophobic magnetic cotton fabricated under low carbonization temperature for effective oil/water separation[J]. *Separation and Purification Technology*, **2021**, *266*: 118535.
53. Liu M, Tan X, Li X, et al. Transparent superhydrophobic EVA/SiO_2/PTFE/KH-570 coating with good mechanical robustness, chemical stability, self-cleaning effect and anti-icing property fabricated by facile dipping method[J]. *Colloids and Surfaces A: Physicochemical and Engineering Aspects*, **2023**, *658*: 130624.
54. Yang J, He T, Li X, et al. Rapid dipping preparation of superhydrophobic TiO_2 cotton fabric for multifunctional highly efficient oil-water separation and photocatalytic degradation[J]. *Colloids and Surfaces A: Physicochemical and Engineering Aspects*, **2023,** *657*: 130590.
55. Luo M, Sun X, Zheng Y, et al. Non-fluorinated superhydrophobic film with high transparency for photovoltaic glass covers[J]. *Applied Surface Science*, **2023**, *609*: 155299.
56. Yao T, Song J, Gan Y, et al. Preparation of cellulose-based chromatographic medium for biological separation: A review[J]. *Journal of Chromatography A*, **2022,** *1677*: 463297.
57. Wang W, Dong C, Liu S, et al. Super-hydrophobic cotton aerogel with ultra-high flux and high oil retention capability for efficient oil/water separation[J]. *Colloids and Surfaces A: Physicochemical and Engineering Aspects*, **2023**, *657*: 130572.
58. Wang H, Meng J, Li F, et al. Graphitic carbon nitride/metal-organic framework composite functionalized cotton for efficient oil-water separation and dye degradation[J]. *Journal of Cleaner Production*, **2023**, *385*: 135758.
59. Cassie A B D, Baxter S. Wettability of porous surfaces[J]. *Transactions of the Faraday society*, **1944**, *40*: 546-551.
60. Qin L, Liu Z, Liu T, et al. A bioinspired, strong, all-natural, superhydrophobic cellulose-based straw[J]. *International Journal of Biological Macromolecules*, **2022**, *220*: 910-919.
61. Xu Y, Yu Y, Song C, et al. One-step preparation of efficient SiO_2/PVDF membrane by sol-gel strategy for oil/water separation under harsh environments[J]. *Polymer*, **2022**, *260*: 125402.
62. Zhang Y, Zhang Y, Cao Q, et al. Novel porous oil-water separation material with super-hydrophobicity and super-oleophilicity prepared from beeswax, lignin, and cotton[J]. *Science of the Total Environment*, **2020**, *706*: 135807.
63. Wen H, Raza S, Wang P, et al. Robust super hydrophobic cotton fabrics functionalized with Ag and PDMS for effective antibacterial activity and efficient oil–water separation[J]. *Journal of Environmental Chemical Engineering*, **2021**, *9(5)*: 106083.

 doi:10.20944/preprints202304.0357.v1

64. Li F, Bhushan B, Pan Y, et al. Bioinspired superoleophobic/superhydrophilic functionalized cotton for efficient separation of immiscible oil-water mixtures and oil-water emulsions[J]. *Journal of colloid and interface science*, **2019**, *548*: 123-130.